Nuclear Physics B130 (1977) 76–92


# DYNAMICAL DETERMINATION OF PARTON AND GLUON DISTRIBUTIONS IN QUANTUM CHROMODYNAMICS

M. GLÜCK and E. REYA
*Institut für Physik, Universität Mainz, 6500 Mainz, West Germany*

Received 15 June 1977

Using the dynamical assumption that at low resolution-energies hadrons consist of valence quarks only, we calculate uniquely nucleonic as well as pionic parton and gluon distributions within the framework of QCD, and give analytic expressions for their $x$- and $Q^2$-dependence. Applications to dilepton and W-boson Drell-Yan production in pN and $\pi$N reactions are illustrated and possible applications to high-$p_T$ processes are discussed.

## 1. Introduction

Parton distributions in nucleons are experimentally obtainable in deep inelastic lepton-nucleon scattering processes. Specifically the antiquark distributions afford detailed knowledge of neutrino and antineutrino cross sections in addition to the accurately measured [1] electroproduction structure functions. As a result of the scarce neutrino data, antiquark ("sea") distributions in nucleons are not well known. This is reflected in the many parametrizations of the sea [2–7] differing in their shape at $x \lesssim 1$ as well as in their normalization at $x = 0$. From neutrino experiments one further learns [8] that about 50% of the nucleon momentum is carried by a flavor neutral component – the "gluon". Because of their flavor neutrality the gluons do not contribute directly to leptonic structure functions and are therefore not directly measurable in the above mentioned experiments.

A possible way to *theoretically* determine the gluon and antiquark content of the nucleon is to imagine [4] the nucleon to consist essentially of its constituent ("valence") quarks. The gluons are then generated through bremsstrahlung off the constituent quarks. Part of the so produced gluons materialize into quark-antiquark pairs – the sea.

To make a specific prediction one has to assume [9] that for a sufficiently low resolution ($Q^2 \equiv -q^2 = \mu^2 \simeq 0.1 - 0.5$ GeV$^2$) of the nucleon structure, the nucleon looks like a pure 3-valence-quark system. Only for $Q^2 > \mu^2$ is the gluon and sea structure then assumed to be discernible. This physically very plausible dynamical boundary condition enables one to express, with the help of well-known renormalization group techniques, *all* distributions in terms of the *two* (up and down) valence distri-

butions at $Q^2 = \mu^2$. Hence the *four* unknown distributions (up and down valence, sea, gluons) are uniquely calculable if *two* independent input structure functions, say $F_2^{ep,n}$ measured at $Q^2 = Q_0^2 >> \mu^2$ are experimentally available.

It should be emphasized that such a unique calculation of parton and gluon distributions, based on the conventional dressing idea of renormalizable field theories, can only be done within the framework of asymptotically free gauge theories (AFGT). This is because the assumption that at very low values of $Q^2$ the nucleon consists of valence quarks only, leads to theoretical and experimental inconsistencies in all asymptotically non-free theories [10]. Furthermore, there are strong indications that AFGT is the only theory compatible with present data on scaling deviations [10,11].

A similar calculation can be undertaken for parton and gluon distributions in the pion. Here (because of charge conjugation and isospin symmetry) only *one* unknown input valence distribution exists and is needed as input. However, due to the fact that deep inelastic scattering data off pion targets are unavailable, one can fix the unknown valence distribution only indirectly using some indications [7] from high-$p_T$ hadron scattering data, hadronic dilepton production data [12,13], and/or theoretical prejudices based on common Regge and counting-rule lore [5].

In sect. 2 the details of the theoretical calculations are presented as well as the underlying assumptions. In sect. 3 we discuss the resulting numerical predictions for nucleonic and pionic parton and gluon distributions and give explicit analytic expressions for their $x$- as well as $Q^2$-dependence. In sect. 4 a few applications to hadronic dilepton and W-boson production using the Drell-Yan mechanism are illustrated and possible applications to high-$p_T$ inclusive hadron reactions are suggested and discussed in sect. 5 where our conclusions are summarized.

## 2. Calculation of parton and gluon distributions

### *2.1. Nucleon distributions*

Let $u_V$, $d_V$, $\xi$ and $G$ denote the up-, down-valence, sea and gluon distributions in the proton, respectively, with the common decomposition $u = u_V + \xi$, $d = d_V + \xi$ and $\bar{u} \simeq \bar{d} \simeq s \simeq \bar{s} \equiv \xi$, which are functions of the scaling variable $x = \omega^{-1} = Q^2/2M\nu$ and of $Q^2$. Decomposing [11] these distributions into (flavor) singlet and non-singlet pieces, and using for the latter the $Q^2$ dependence as predicted by the renormalization group [14,11], the assumption [9] $x\xi(x, Q^2 = \mu^2) = xG(x, Q^2 = \mu^2) = 0$ leads to

$$\langle xu_V(Q_0^2)\rangle_n = \langle xu_V(\mu^2)\rangle_n L_0^{-a_{NS}}\,, \tag{1}$$

$$\langle xd_V(Q_0^2)\rangle_n = \langle xd_V(\mu^2)\rangle_n L_0^{-a_{NS}}\,, \tag{2}$$

$$\langle x\xi(Q_0^2)\rangle_n = \tfrac{1}{6}\langle xu_V(\mu^2) + xd_V(\mu^2)\rangle_n [p_{\bar{1}1} L_0^{-a_-} + (1 - p_{\bar{1}1}) L_0^{-a_+} - L_0^{-a_{NS}}]\,, \tag{3}$$

$$\langle xG(Q_0^2)\rangle_n = \langle xu_V(\mu^2) + xd_V(\mu^2)\rangle_n (1 - \bar{p}_{11}) \frac{\bar{p}_{11}}{\bar{p}_{21}} [L_0^{-a_-} - L_0^{-a_+}] , \tag{4}$$

where the moments are defined by $\langle f(Q^2)\rangle_n \equiv \langle f(x, Q^2)\rangle_n \equiv \int_0^1 dx\, x^{n-2} f(x, Q^2)$, and $L_0 \equiv L(Q_0^2)$ with

$$L \equiv L(Q^2) \equiv \frac{\bar{\alpha}(\mu^2)}{\bar{\alpha}(Q^2)} = \frac{\ln(Q^2/\Lambda^2)}{\ln(\mu^2/\Lambda^2)} . \tag{5}$$

Using a SU(3) flavor group the running coupling constant is given by $\bar{\alpha} \equiv \bar{g}^2/4\pi = 4\pi/9\ln(Q^2/\Lambda^2)$. The quantities $a_i = a_i(n)$, $\bar{p}_{ij} = \bar{p}_{ij}(n)$ and $\Lambda$ are the standard [14] anomalous dimensions, singlet projection matrix elements and the mass scale, respectively, where we closely follow the notation of ref. [11]. Recalling

$$F_2^{eN} \equiv \tfrac{1}{2}(F_2^{ep} + F_2^{en}) = \tfrac{5}{18}(xu_V + xd_V) + \tfrac{4}{3}x\xi \tag{6}$$

and substituting eqs. (1)–(3) into it, one obtains

$$\langle xu_V(\mu^2) + xd_V(\mu^2)\rangle_n = \frac{18\langle F_2^{eN}(Q_0^2)\rangle_n}{4\bar{p}_{11}L_0^{-a_-} + 4(1 - \bar{p}_{11})L_0^{-a_+} + L_0^{-a_{NS}}} . \tag{7}$$

Thus, according to eqs. (3) and (4), $\xi(x, Q_0^2)$ and $G(x, Q_0^2)$ are uniquely determined in terms of $F_2^{eN}(x, Q_0^2)$ once $L_0$ (or $\mu^2$) is given. For this purpose recall that energy-momentum conservation implies

$$\langle xu_V(Q^2)\rangle_2 + \langle xd_V(Q^2)\rangle_2 + 6\langle x\xi(Q^2)\rangle_2 + \langle xG(Q^2)\rangle_2 = 1 \tag{8}$$

for all $Q^2$. In particular, at $Q^2 = \mu^2$ where $\xi = G = 0$ one has

$$\langle xu_V(\mu^2)\rangle_2 + \langle xd_V(\mu^2)\rangle_2 = 1 . \tag{9}$$

Taking $n = 2$ in eq. (7) and using (9) one obtains

$$\langle F_2^{eN}(Q_0^2)\rangle_2 = \tfrac{2}{9}(\tfrac{9}{25} + \tfrac{16}{25}L_0^{-50/81}) + \tfrac{1}{18}L_0^{-32/81} . \tag{10}$$

Experimentally [1,15] $\langle F_2^{eN}(Q_0^2 \simeq 3\ \mathrm{GeV}^2)\rangle_2 = 0.15 \pm 0.01$, which implies $L_0 = 7 \pm 2$.

Having obtained $L_0$, $\langle xu_V(\mu^2) + xd_V(\mu^2)\rangle_n$ is now uniquely determined by eq. (7), and with it all parton and gluon distributions at $Q_0^2$ through eqs. (1)–(4). To separate $u_V(x, \mu^2)$ from $d_V(x, \mu^2)$ one further uses

$$F_2^{ep}(x, Q_0^2) - F_2^{en}(x, Q_0^2) = \tfrac{1}{3}[xu_V(x, Q_0^2) - xd_V(x, Q_0^2)] \tag{11}$$

together with eqs. (1), (2) and (7). The distributions at $Q^2 > Q_0^2$ are now obtainable by replacing in eqs. (1)–(4) $Q_0^2 \to Q^2$, $L_0 \to L = L_0\ln(Q^2/\Lambda^2)/\ln(Q_0^2/\Lambda^2)$.

Above and also throughout our analysis we have taken the mean experimental momentum transfer $Q_0^2$ to be $Q_0^2 = 3 \pm 1\ \mathrm{GeV}^2$ which corresponds to the measurements presented in refs. [1,8,15], except close to threshold ($x \simeq 1$) where we appropriately

correct the input data as discussed in the next section. This, together with [9,11,16, 17] 300 MeV $\lesssim \Lambda \lesssim$ 600 MeV implies 350 MeV $\lesssim \mu \lesssim$ 700 MeV, i.e., the resolution size at which only constituent-valence structure is observed coincides approximately with the mass scale $\Lambda$ and with the average momentum of the quarks inside a nucleon at rest.

To calculate the charm-sea $c = \bar{c} \equiv \xi'$ component of the nucleon one has to extend the above analysis to the SU(4) flavor group. Because of the large SU(4) symmetry breaking ($m_c^2 >> m_u^2 \simeq m_d^2 \simeq m_s^2 \simeq 0$), $\xi' \neq \xi$, one must keep $m_c^2/Q^2$ corrections [18] which unfortunately are not yet fully understood because of their possible dependence on long-range strong interaction effects [19]. It will be certainly worthwhile to undertake this very lengthy and cumbersome numerical analysis, once these problems are settled. On the other hand the large mass ratio of charmed to uncharmed quarks enables one to treat the light quark distributions separately, because of their small mixing with heavy quarks.

### 2.2. Pion distributions

The pion consists of only two constituents of which one is an antiquark. Because of isospin and charge conjugation symmetry one has

$$u^{\pi^+} = \bar{d}^{\pi^+} = \bar{u}^{\pi^-} = d^{\pi^-} \equiv v^\pi + \xi^\pi ,$$

$$\bar{u}^{\pi^+} = d^{\pi^+} = u^{\pi^-} = \bar{d}^{\pi^-} \simeq s^{\pi^\pm} = \bar{s}^{\pi^\pm} \equiv \xi^\pi \tag{12}$$

with $v^\pi$ and $\xi^\pi$ the valence and sea components, respectively. Assuming as before that $x\xi^\pi(x, Q^2 = \mu^2) = xG^\pi(x, Q^2 = \mu^2) = 0$, one obtains

$$\langle xv^\pi(Q^2)\rangle_n = \langle xv^\pi(Q_0^2)\rangle_n (L/L_0)^{-a_{\rm NS}} , \tag{13}$$

$$\langle x\xi^\pi(Q^2)\rangle_n = \tfrac{1}{3}\langle xv^\pi(Q_0^2)\rangle_n L_0^{a_{\rm NS}} [p_{11}^- L^{-a_-} + (1 - p_{11}^-) L^{-a_+} - L^{-a_{\rm NS}}] , \tag{14}$$

$$\langle xG^\pi(Q^2)\rangle_n = 2\langle xv^\pi(Q_0^2)\rangle_n L_0^{a_{\rm NS}} (1 - p_{11}^-) \frac{p_{11}^-}{p_{21}^-} [L^{-a_-} - L^{-a_+}] . \tag{15}$$

One sees that knowledge of only *one* input function at $Q_0^2$ and of $L_0$ uniquely determines all other distributions. Experimental data on the $\pi$ structure are however scarce and only indirectly obtainable, since deep inelastic lepton-pion data are not available. The only available (indirect) data consist of massive dilepton production in $\pi$N scattering [12,13], and of high-$p_T$ $\pi$N inclusive hadron production [20]. Extraction of the pion structure function from these data is highly model dependent [7] and therefore insecure, so one has to use, in addition, some theoretically biased assumptions [5,7] to fix, say, $v^\pi(x, Q_0^2)$. For example the common lore on counting rules and Regge behavior suggests [5]

$$xv^\pi(x, Q_0^2) = \tfrac{3}{4}\sqrt{x}(1 - x) , \tag{16}$$

where the normalization is fixed by the baryon number constraint $\langle xv^{\pi}(Q^2)\rangle_1 = 1$.

Using the Drell-Yan-West relation to connect the deep inelastic structure function near $x = 1$ and elastic form factors, and taking into account that the pion has spin zero, Feynman and Field [7] argue that $xv^{\pi}(x, Q_0^2)$ need not vanish as $x \to 1$ and suggest $xv^{\pi}(x = 1, Q_0^2) \simeq \frac{1}{4}$. Taking a simple form like

$$xv^{\pi}(x, Q_0^2) = c\sqrt{x}(b - x) , \tag{17}$$

yields, together with $\langle xv^{\pi}(Q^2)\rangle_1 = 1$, $c = \frac{3}{8}$ and $b = \frac{5}{3}$.

We shall confront both forms (16) and (17) with dilepton production data [12, 13] and observe a slight preference of the Feynman-Field suggestion. Therefore, in the sequel we will mainly concentrate on the consequences of using the latter input structure function and on their respective analytic representations. It should be emphasized, however, that *total* $\mu^+\mu^-$ production cross sections are not an ideal test for the detailed $x$-behavior of parton distributions. The only remaining free parameter $L_0$ is fixed by the requirement that at $Q^2 = \mu^2$ the two valence quarks carry all of the pion's momentum, i.e., $1 = \langle 2xv^{\pi}(\mu^2)\rangle_2 = \langle 2xv^{\pi}(Q_0^2)\rangle_2 \exp(\frac{32}{81} \ln L_0)$. This yields $L_0 = 10.17$ for the Farrar-like input of eq. (16), and $L_0 = 4.91$ for the Feynman-Field-like input of eq. (17).

## 3. Predictions for parton distributions

### *3.1. Nucleon distributions*

Using standard Mellin inversion techniques [9,16], the various parton and gluon distributions in the nucleon at arbitrary $Q^2$ can be uniquely calculated once the input functions $F_2^{ep,n}(x, Q_0^2)$ in eqs. (7) and (11) are given. For these we use [1]

$$F_2^{ep}(x, Q_0^2 \simeq 3\ \mathrm{GeV}^2) = 3.033(1 - x)^3 - 3.351(1 - x)^4 + 0.518(1 - x)^5,$$

$$F_2^{en}/F_2^{ep} = 1 - 1.135x + 0.385x^2 . \tag{18}$$

Since the data for $F_2^{ep}$ correspond to $Q^2 \simeq 10\ \mathrm{GeV}^2$ for $x > 0.25$, we have corrected (increased) the threshold measurements of Miller et al. [1] by using the AFGT threshold formula of Gross [21]

$$\frac{F_2^{ep}(x, 3\ \mathrm{GeV}^2)}{F_2^{ep}(x, 10\ \mathrm{GeV}^2)} = 1.276\ (-\ln x)^{-0.219} , \tag{19}$$

which is valid for $x \gtrsim 0.3$. Fig. 1 shows the predictions for the momentum distributions within the nucleon. Taking into account the uncertainties of the input parameters and data, which on the average amount to a 30% ambiguity of the theoretical predictions, we obtain already for $Q^2 \simeq 1\ \mathrm{GeV}^2$ good agreement with the experimental result [8] that at low values of $Q^2$ about 50% of the nucleon momentum is carried

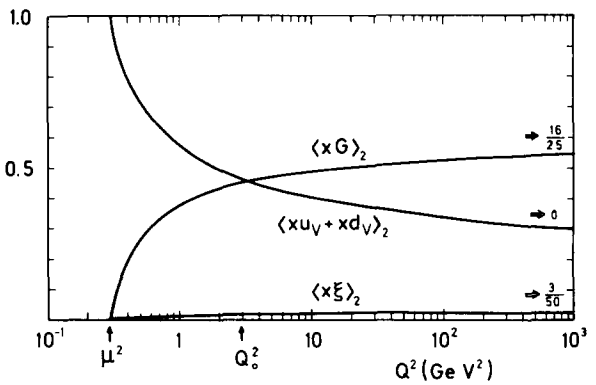


Fig. 1. AFGT predictions for the momentum distributions within the nucleon. The "static point" $\mu^2 = 0.3$ GeV$^2$ corresponds to $\Lambda = 0.45$ GeV, for a given $L_0 = 7$ and $Q_0^2 = 3$ GeV$^2$.

by gluons. This gives us some confidence in these dynamical predictions as long as $Q^2 \gtrsim 1$ GeV$^2$, whereas predictions for $Q^2 < 1$ GeV$^2$ are clearly not to be taken seriously due to the strong variations in this region as shown in fig. 1.

The predictions for the full $x$- as well as $Q^2$-dependence of valence, sea, and gluon distributions are shown in figs. 2 and 3. The shaded areas correspond to the ambiguities of the input data [1] in eq. (18) as well as of the input parameters ($L_0 = 7 \pm 2$, $\Lambda = 0.45 \pm 0.15$ GeV, $Q_0^2 = 3 \pm 1$ GeV$^2$). Since for practical purposes it is not very useful to have the $x$- and $Q^2$-dependence of densities in a numerical form only, we have instead represented them as simple analytic expressions by parametrizing the $x$-dependence in powers of $(1 - x)$, and the $Q^2$ dependence in a form similar to that predicted by AFGT. We have fitted these parametrizations to the AFGT predictions using as input $L_0 = 7$, $\Lambda = 0.45$ GeV, and $Q_0^2 = 3$ GeV$^2$. The solid and dashed curves in figs. 2 and 3 are typical results of these parametrizations, which are summarized in the appendix. (It should be emphasized that, according to the input uncertainty a typical error of ±20% should be attached to all "unique" parametrized predictions.) In fig. 3 we compare our predictions for the sea $x\xi$ with the two extreme parametrizations proposed in the *naive* quark-parton model which should hold for 2 GeV$^2 \lesssim Q^2 \lesssim 10$ GeV$^2$: Although the Barger-Phillips sea [3] as well as all other parametrizations [5,6] compatible with naive counting rules [22], $x\xi \simeq 0.1(1 - x)^7$, do on the average (surprisingly) agree with our field theoretic predictions for $x \lesssim 0.6$, the modified Kuti-Weisskopf (MKW) parametrization [2] disagrees by about two orders of magnitude for $x > 0.2$. Besides this field theoretic prejudice against the MKW sea, we have no hard experimental evidence against MKW but we shall come back to this point in the next section.

Our analytic expressions (A.1) can be directly compared with naive counting rules [22] where the threshold suppression of a $n$-constituent state distribution function is expected to be $(1 - x)^{2n-3}$: whereas the valence ($n = 3$) and gluon

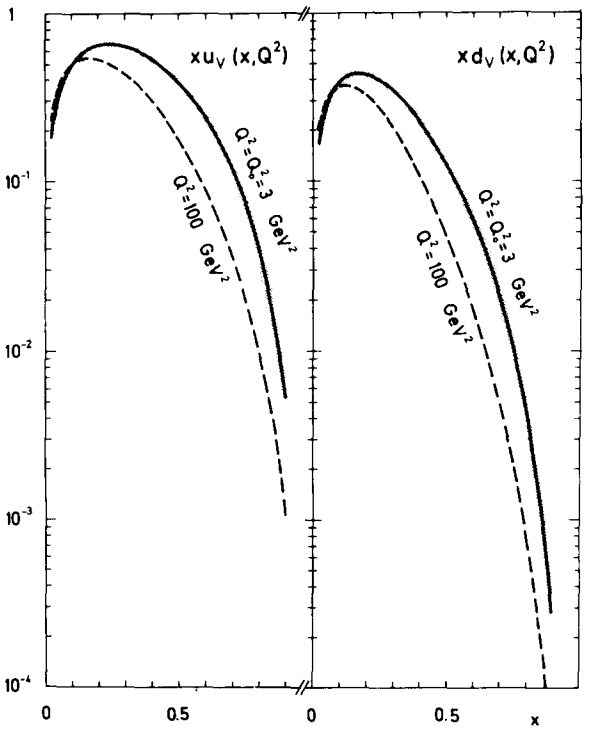


Fig. 2. Predictions for the valence-quark distributions within the nucleon. The shaded area corresponds to the uncertainty of our predictions due to the ambiguities of the input data. The solid curves are the fits, eq. (A.1), to the AFGT predictions for $L_0 = 7$, $Q_0^2 = 3$ GeV$^2$ and $\Lambda = 0.45$ GeV. The dashed lines are the corresponding distributions at $Q^2 = 100$ GeV$^2$.

($n = 4$) densities in (A.1) agree with this simple rule, the sea distribution does not fall off as sharply as expected for $n = 5$, i.e., $x\xi \sim (1-x)^7$. This conclusion is characteristic to AFGT predictions for the large $x$-region, and moreover it appears unlikely that taking care of threshold effects [17,18] could account for the missing two orders of magnitude.

In fig. 4 we compare our predictions for the quark- and antiquark-densities $q$ and $\bar{q}$, respectively, at $Q^2 = 3$ GeV$^2$ with experiment. In view of the rather poor data and the 30% uncertainty to be attached to the theoretical curves, the agreement is satisfactory.

### *3.2. Pion distributions*

As already anticipated at the end of sect. 2.2 we will find, by studying Drell-Yan production of dileptons in pp and $\pi$p scattering, a slight preference of the pionic

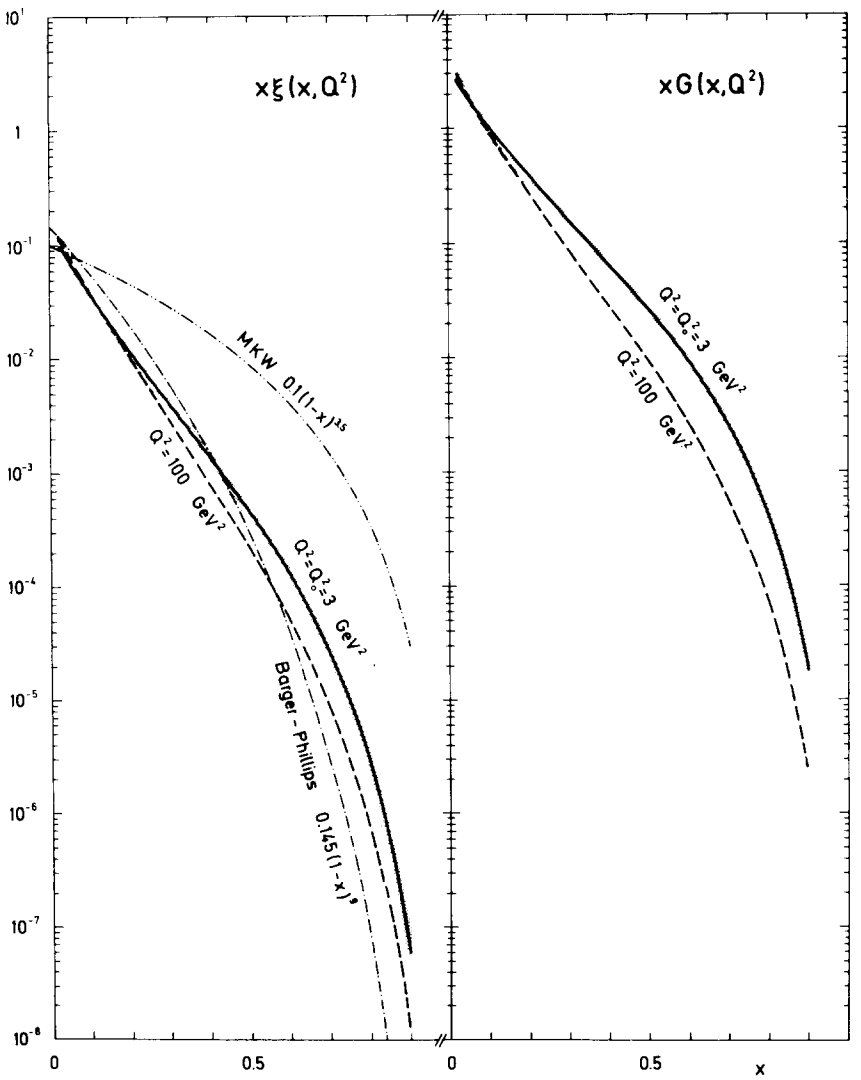


Fig. 3. Predictions for the sea and gluon component of the nucleon, with a notation as in fig. 2. For comparison we also show the two extreme sea parametrizations of naive quark-parton models, the one of Barger and Phillips [3] and the MKW [2].

valence distribution in eq. (17) suggested by Feynman and Field [7] to the one suggested by Farrar [5] in eq. (16). Therefore we give the various analytic parametrizations of $\xi^{\pi}(x, Q^2)$ and $G^{\pi}(x, Q^2)$ as predicted by AFGT in eqs. (13) and (14) only for the input of eq. (17), although we will explicitly compare and discuss in the next section the predictions for dilepton production using the Farrar input eq. (16) as well. These

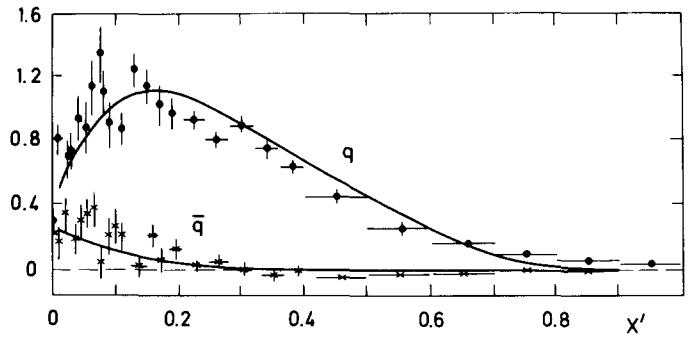


Fig. 4. Comparison of the predicted amounts of quarks $q = xu + xd = x(u_V + d_V + 2\xi)$ and antiquarks $\bar{q} = x\bar{u} + x\bar{d} = 2x\xi$ at $Q^2 = Q_0^2 = 3$ GeV$^2$ with the data [8].

analytic expressions are summarized in eqs. (A.4) and (A.5), from which it is obvious that the threshold behavior of the gluon as well as of the sea are inconsistent with naive expectations using dimensional analysis [22], i.e., $xG^\pi \sim (1-x)^3$ and $x\xi^\pi \sim (1-x)^5$ for $n = 3$ and $n = 4$, respectively.

## 4. Hadronic dilepton and $W^\pm$ production

Application of dynamically calculated parton distributions to scaling violations of structure functions were already successfully undertaken in ref. [9] for $\partial \ln F_2^{ep}/\partial \ln Q^2$. We will therefore test these distributions in another context namely that of heavy dilepton production in hadronic collisions. Here one imagines a parton (antiparton) with a fraction $x_A$ of the incoming particle A annihilating an antiparton (parton) of fractional momentum $x_B$ in the target B, thereby creating a heavy virtual photon which then decays into the lepton pair (Drell-Yan mechanism [23]). The cross section for creating in this way dileptons of mass $m$ is given by (the factor $\frac{1}{3}$ is due to color)

$$\frac{d\sigma}{dQ^2} = \frac{1}{3}\frac{4\pi\alpha^2}{3Q^4}\int \frac{dx_A}{x_A} G^{AB}(x_A, Q^2) \tag{20}$$

with $Q^2 \equiv m^2$, and

$$G^{AB}(x_A, Q^2) = x_A x_B \sum_i e_i^2 \{q_i^A(x_A, Q^2)\, q_{\bar{i}}^B(x_B, Q^2) + i \leftrightarrow \bar{i}\}, \tag{21}$$

where $e_i$ is the charge of the parton $i$ and $q_i^A$ stands for the distribution of partons of type $i$ in A, i.e., $q_u^p \equiv u$, $q_{\bar{s}}^{\pi^+} \equiv \bar{s}^{\pi^+}$, etc., and $x_B$ is related to $x_A$ through

$$x_B = \frac{Q^2}{2M_B p_{lab} x_A} \tag{22}$$

with $2M_B p_{lab} \simeq s$. The integration in eq. (20) is constrained by $0 \leqslant x_{A,B} \leqslant 1$ and $x_A \geqslant Q_L^{min}/p_{lab}$ with $Q^{min}$ being the experimental cutoff of the longitudinal dilepton momentum $Q_L$.

The cross section for creating dileptons of mass $Q^2$ and a definite $Q_L$ is given by

$$\frac{d^2\sigma}{dQ^2 dx_F} = \frac{1}{3}\frac{4\pi\alpha^2}{3Q^4}\frac{1}{x_A + x_B} G^{AB}(x_A, Q^2) \tag{23}$$

with $x_F \equiv x_A - x_B$ and $x_{A,B} = \frac{1}{2}[\pm x_F + (x_F^2 + 4Q^2/s)^{1/2}]$. One might wonder whether the $Q^2$ dependence of $G^{AB}(x_A, Q^2)$ is indeed the one given by eq. (21). Plausibility arguments for the validity of (21) were given in ref. [24] although, in particular for AFGT, the question is not rigorously settled yet [25]. Here, for the lack of better knowledge, eq. (21) will be adopted which allows us to test our predictions for parton distributions and their $Q^2$ dependence. In particular $G^{AB}(x_A, Q^2)$ is directly proportional to the antiquark distribution thereby providing, in principle, a very sensitive test for our predicted sea. Unfortunately all experiments were done on heavy nuclear targets in order to enhance, the otherwise small, production rates. Since, as we shall see, collective nuclear effects are quite important, the existing data does not provide, in practice, a clear cut test for our predictions. This is illustrated in fig. 5 where our predictions (solid and dashed curves), with collective effects neglected, for the low energy experiments on uranium targets [26] are seen to lie much below the data. Similar results are obtained for all other presently known distributions [3,5–7] which agree roughly with our field theoretic predictions, except for the MKW one [2] whose sea is much greater than that of the other distributions (see fig. 3). Such an abnormally huge sea seems to be in conflict with presently available data on antineutrino cross sections [8]. A similar pattern, shown in fig. 6, is obtained for the high energy experiments on copper targets [27]. Since these experiments are not sensitive to the threshold (large $x$) region, contrary to the low energy data [26] in fig. 5, the discrepancy is not as drastic as in fig. 5.

In both cases the inclusion of collective nuclear effects [28] enhances the cross section so as to bring the small sea predictions into the observed region, as shown by the dotted curves of figs. 5 and 6. If one believes the nuclear enhancement calculations [28] based on the collective tube model (CTM), one can conclude that the MKW distributions are excluded by the data since, taken together with collective nuclear effects, they predict a much too large dilepton production rate. It should be emphasized that, besides this alternative, there seems to be little room within the parton model picture for other explanations of the data since different dilepton production mechanisms, like heavy photon bremsstrahlung in quark-quark or quark-gluon scattering, are strongly suppressed [23].

To test our predictions for the pionic parton distributions we now turn to the processes $\pi^{\pm}N \to \mu^+\mu^- + X$. In order to get rid of the strong dependence on possible collective nuclear effects we concentrate on the beam ratios $\sigma(\pi^+)/\sigma(p)$ and $\sigma(\pi^+)/\sigma(\pi^-)$ as measured by the Chicago-Princeton group [13]. For $\sigma(\pi^+)/\sigma(p)$ in

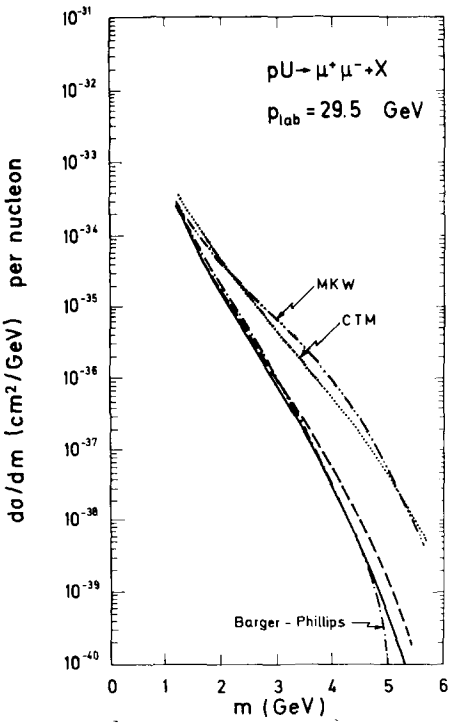


Fig. 5. Resonance subtracted dilepton production data [26] (shaded area – corresponding to an $A^1$ dependence of the nuclear cross section) compared with Drell-Yan model predictions using: a) $Q^2$ *dependent* parton distributions of eq. (A.2) (solid curve); b) $Q^2$ independent parton distributions of eq. (A.1) (dashed curve); c) Barger-Phillips distributions [3]; d) MKW distributions [2]; e) Barger-Phillips-like distributions combined with collective nuclear enhancement (CTM) effects [28].

fig. 7 one notes a slightly better agreement for the pion distributions based on the Feynman-Field input in eq. (17) (solid and dashed curves) than for the Farrar input in eq. (16) as shown by the dotted curves. Using these pionic Feynman-Field-like distributions, eq. (A.4), the data also seem to disfavor the MKW parton distributions in the nucleon, but the large errors in the data as well as the results for $\sigma(\pi^+)/\sigma(\pi^-)$ in fig. 7 prohibit us from drawing any clear cut conclusions. As soon as better and more detailed $\pi$-beam data become availabe, a full analysis including collective target effects will certainly be meaningful and necessary.

Perhaps even more speculative are similar conclusions [29] against the MKW sea drawn from inclusive particle ratios of high-$p_T$ pp reactions. Here a rapidly decreasing sea, $x\xi \sim (1-x)^{5.5}$, seems to be required in order to explain the decrease of $K^-/\pi^-$ and $\bar{p}/\pi^-$ with $p_T$.

Finally, in fig. 8 we present our predictions for $W^+$ production rates in pp colli-

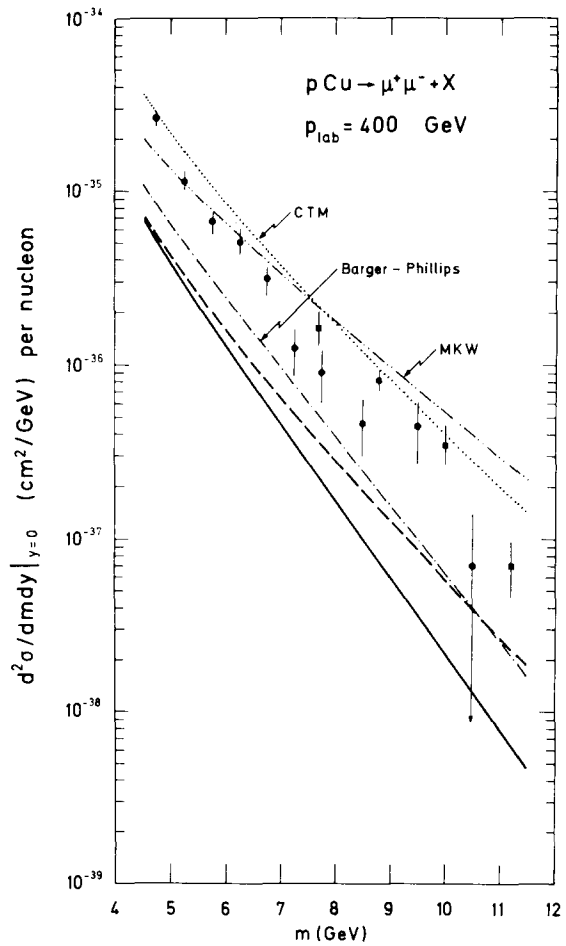


Fig. 6. Comparison of theoretical predictions (notation as in fig. 5) with the high-energy data [27] of Hom et al. (•) and Kluberg et al. (▪), where $y$ denotes the usual center-of-mass rapidity with $x_F \simeq 2my/\sqrt{s}$ for $y \simeq 0$.

sions assuming an underlying Drell-Yan mechanism which yields the cross section

$$\sigma^{W^+} = \tfrac{1}{3}\sqrt{2}\pi G \cos^2\theta_C \int_{M_W^2/s}^{1} \frac{dx_1}{x_1} G_{W^+}^{pp}(x_1, M_W^2)\,, \tag{24}$$

where $\theta_C$ is the Cabibbo angle, and

$$G_{W^+}^{pp}(x_1, M_W^2) = x_1 x_2 [u(x_1, M_W^2)\bar{d}(x_2, M_W^2) + \bar{d}(x_1, M_W^2) u(x_2, M_W^2)] \tag{25}$$

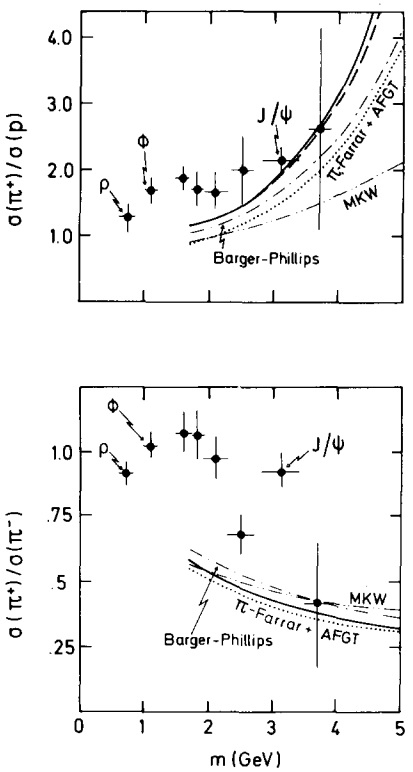


Fig. 7. Beam ratio data [13] for $\mu^+\mu^-$ production ($x_F > 0$) on Carbon at 225 GeV/$c$ as compared to Drell-Yan model predictions using: a) $Q^2$ dependent pion and nucleon distributions of eqs. (A.5) and (A.2) (solid lines); b) $Q^2$ independent pion and nucleon distributions of eqs. (A.4) and (A.1) (dashed lines – which coincides with the solid curve for $\sigma(\pi^+)/\sigma(\pi^-)$); c) $Q^2$ independent pion distributions of eq. (A.4) with the nucleonic Barger-Phillips distributions (dashed-dotted lines); d) pion distributions as in c) together with nucleonic MKW distributions (dashed-double dotted lines); e) $Q^2$ independent pionic distributions resulting from the Farrar input eq. (16) together with the nucleonic distributions of eq. (A.1) (dotted lines). Using in c) and d) the pionic Farrar-like distributions instead, reduces the corresponding curves by 30% for $\sigma(\pi^+)/\sigma(p)$ and by 5% for $\sigma(\pi^+)/\sigma(\pi^-)$.

with $x_2 = M_W^2/sx_1$. We have calculated this cross section only for $M_W^2/s \gtrsim 0.1$ where contributions from the charmed sea are negligible, using $M_W^2 = 4000$ GeV$^2$. From fig. 8 it is clear that W-boson production will be a very sensitive test for the sea component: Whereas AFGT corrections (solid curve) reduce the predictions of almost all naive quark-parton models (dashed and dashed-dotted curves) by about one order of magnitude, the naive MKW distributions yield production rates three orders of magnitude larger than expected from AFGT.

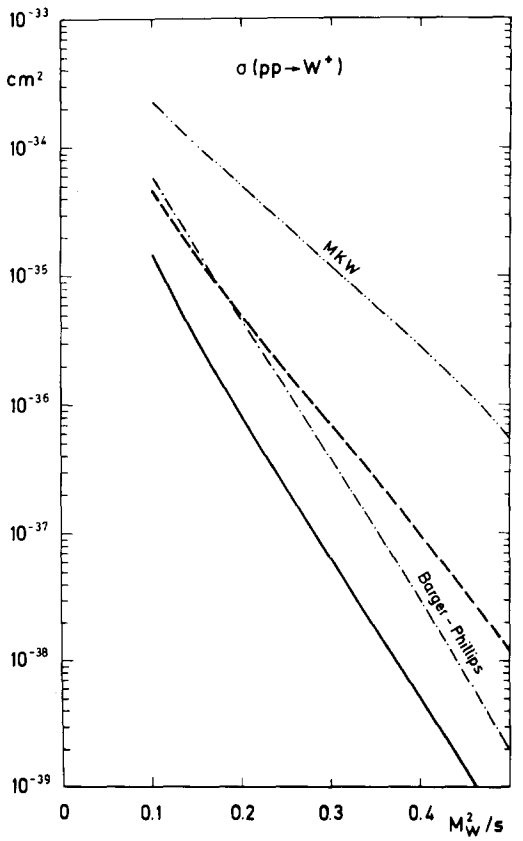


Fig. 8. Predictions for $W^+$ production in pp collisions using the $Q^2$ dependent distributions of eq. (A.3) (solid curve), and the $Q^2$ independent distributions of eq. (A.1) (dashed curve). The latter should be compared with the predictions obtained by using Barger-Phillips and MKW densities.

## 5. Conclusions

Using the dynamical assumption that at low resolution-energies $Q^2$ hadrons consist of valence quarks only, we have uniquely calculated nucleonic as well as pionic parton and gluon distributions using renormalization group techniques. For practical purposes we give also analytic expressions for the $x$- and $Q^2$-dependence of these densities. Although these field theoretic predictions agree on the average well with almost all parametrizations of nucleonic parton distributions of naive quark-parton models [3,5–7], apart from slight discrepancies in the threshold behavior when compared with naive counting rules, they are totally incompatible with the huge sea component of the modified Kuti-Weisskopf (MKW) parametrization [2]. Besides this field theo-

retic prejudice against the MKW sea, we have no conclusive experimental evidence against it.

Applying these nucelonic and pionic distributions to the dilepton production in pN and $\pi$N collisions, our predictions as well as those of all other naive (colored) parton models, except MKW, lie below the data for $pN \to \mu^+\mu^- + X$. The agreement of MKW, however, might be illusory since collective nuclear effects can account very well for the data without using the huge MKW sea, which seems to be in conflict with presently available data on neutrino and antineutrino cross sections. Furthermore the beam ratios $\sigma(\pi^+)/\sigma(p)$ and $\sigma(\pi^+)/\sigma(\pi^-)$ for $\mu^+\mu^-$ production seem to disfavor the MKW parton distributions in the nucleon and to prefer slightly pionic parton distributions which are based on a Feynman-Field input, i.e. $xu^{\pi^+}(x=1) \neq 0$, instead those based on the usual Farrar-like input $xu^{\pi^+}(x=1) = 0$. The poor statistics of the data, however, prohibit us from drawing any clear cut conclusions. In addition it should be emphasized that, contrary to $x_F$ distributions, *total* dilepton production cross sections are no ideal test for the shape of parton distributions.

Our parton distributions may also be useful in studies of high-$p_T$ hadronic scattering experiments where according to Berman, Bjorken and Kogut [30] the main dynamical mechanism is a hard parton-parton collision. Present extensive studies of this idea consider only the hard quark-quark scattering and neglect the hard quark-gluon and gluon-gluon scattering completely. With our conjectured gluon distributions it is now possible to fill this gap and see whether agreement with experiment is thereby improved, taking also into account the correct $Q^2$ dependence as predicted by AFGT. Specifically one could see whether it is possible to avoid the unusually high quark-gluon coupling constant [7,29] presently introduced in a rather ad hoc way in order to obtain agreement with the data.

## Appendix

Parametrizing the AFGT predictions for the $x$- and $Q^2$-dpendence of the parton and gluon distributions as explained in the text, we obtain the following expressions for the nucleon densities (all $Q^2$'s are to be understood in units of $GeV^2$):

$$xu_V(x, Q_0^2) = \sqrt{x}[5.707(1-x)^3 - 6.219(1-x)^5 + 4.570(1-x)^7 - 2.868(1-x)^9],$$

$$xd_V(x, Q_0^2) = \sqrt{x}[2.994(1-x)^4 - 0.767(1-x)^5 + 1.890(1-x)^7 - 3.026(1-x)^9],$$

$$x\xi(x, Q_0^2) = 0.019(1-x)^{5.5} + 0.007(1-x)^9 + 0.091(1-x)^{13},$$

$$xG(x, Q_0^2) = 0.557(1-x)^{4.5} + 0.559(1-x)^9 + 2.037(1-x)^{13}. \qquad \text{(A.1)}$$

with $Q_0^2 = 3$ and $x \gtrsim 0.03$. The $Q^2$ dependence is given by

$$xu_V(x, Q^2) = xu_V(x, Q_0^2)\left[\frac{\ln(Q^2/3 \times 10^{-6})}{\ln(Q_0^2/3 \times 10^{-6})}\right]^{0.951 - x\ln(Q^2/0.012)},$$

$$xd_V(x,Q^2) = xd_V(x,Q_0^2)\left[\frac{\ln(Q^2/7\times10^{-7})}{\ln(Q_0^2/7\times10^{-7})}\right]^{0.791-x\ln(Q^2/0.0015)},$$

$$x\xi(x,Q^2) = x\xi(x,Q_0^2)\left[\frac{\ln(Q^2/1\times10^{-3})}{\ln(Q_0^2/1\times10^{-3})}\right]^{0.67-x\ln(Q^2/0.583)},$$

$$xG(x,Q^2) = xG(x,Q_0^2)\left[\frac{\ln(Q^2/4\times10^{-5})}{\ln(Q_0^2/4\times10^{-5})}\right]^{0.288-x\ln(Q^2/0.031)}, \qquad \text{(A.2)}$$

which is an accurate representation of the exact AFGT predictions in the range $2\ \text{GeV}^2 \lesssim Q^2 \lesssim 250\ \text{GeV}^2$. The usual valence quark constraints $\int_0^1 u_V dx = 2$ and $\int_0^1 d_V dx = 1$ are satisfied within the quoted uncertainty of ±20%.

For detailed studies of the production of exotica (e.g. $W^{\pm}$, $Z^0$) in hadron-hadron colliding beam experiments, it is useful to know the parton distributions also at $Q^2 = 4000\ \text{GeV}^2$ (corresponding roughly to the size of $M_W^2$ and $M_Z^2$):

$$xu_V(x,4000) = \sqrt{x}[0.463(1-x)^3 + 6.031(1-x)^5 - 8.117(1-x)^7 + 3.965(1-x)^9],$$

$$xd_V(x,4000) = \sqrt{x}[0.109(1-x)^4 + 0.821(1-x)^5 + 2.254(1-x)^7 - 1.418(1-x)^9],$$

$$x\xi(x,4000) = 0.0045(1-x)^{5.8} + 0.0404(1-x)^9 + 0.081(1-x)^{13}. \qquad \text{(A.3)}$$

Proceeding in a similar way for parton densities within the pion, using as input eq. (17), we obtain for $x \gtrsim 0.03$

$$xv^{\pi}(x,Q_0^2) = 0.375\sqrt{x}(1.667-x),$$

$$x\xi^{\pi}(x,Q_0^2) = 0.013(1-x)^{2.5} + 0.007(1-x)^7 + 0.052(1-x)^{11},$$

$$xG^{\pi}(x,Q_0^2) = 0.267(1-x)^{1.5} + 1.459(1-x)^7 + 0.248(1-x)^{11}, \qquad \text{(A.4)}$$

with $Q_0^2 = 3$, and for $2 \lesssim Q^2 \lesssim 250$,

$$xv^{\pi}(x,Q^2) = xv^{\pi}(x,Q_0^2)\left[\frac{\ln(Q^2/1.5\times10^{-7})}{\ln(Q_0^2/1.5\times10^{-7})}\right]^{1.46-\frac{1}{4}x\ln(Q^2/1.8\times10^{-10})},$$

$$x\xi^{\pi}(x,Q^2) = x\xi^{\pi}(x,Q_0^2)\left[\frac{\ln(Q^2/5.8\times10^{-9})}{\ln(Q_0^2/5.8\times10^{-9})}\right]^{3.41-\frac{1}{2}x\ln(Q^2/1.9\times10^{-8})},$$

$$xG^{\pi}(x,Q^2) = xG^{\pi}(x,Q_0^2)\left[\frac{\ln(Q^2/3.4\times10^{-7})}{\ln(Q_0^2/3.4\times10^{-7})}\right]^{0.69-x\ln(Q^2/0.01)}. \qquad \text{(A.5)}$$

Again, an uncertainty of typically ±20% should be assigned to all these predictions.

## References

[1] G. Miller et al., Phys. Rev. D5 (1972) 528;
A. Bodek et al., Phys. Rev. Lett. 30 (1973) 1087;
J.S. Poucher et al., Phys. Rev. Lett. 32 (1974) 118.
[2] R. McElhaney and S.F. Tuan, Phys. Rev. D8 (1973) 2267.
[3] V. Barger and R.J.N. Phillips, Nucl. Phys. B73 (1974) 269.
[4] G. Altarelli, N. Cabibbo, L. Maiani and R. Petronzio, Nucl. Phys. B69 (1974) 531.
[5] G.R. Farrar, Nucl. Phys. B77 (1974) 429.
[6] J.F. Gunion, Phys. Rev. D10 (1974) 242;
G. Chu and J.F. Gunion, Phys. Rev. D10 (1974) 3672;
R. Blankenbecler et al., SLAC-PUB-1513 (1975).
[7] R.D. Field and R.P. Feynman, Phys. Rev. D15 (1977) 2590.
[8] T. Eichten et al., Phys. Lett. 46B (1973) 274;
H. Deden et al., Nucl. Phys. B85 (1975) 269.
[9] G. Parisi and R. Petronzio, Phys. Lett. 62B (1976) 331.
[10] M. Glück and E. Reya, Phys. Lett. 69B (1977) 77.
[11] M. Glück and E. Reya, University of Mainz report MZ-TH 76/10, Phys. Rev. D, to be published.
[12] K.J. Anderson et al., Phys. Rev. Lett. 36 (1976) 237.
[13] K.J. Anderson et al., submitted paper to Tbilisi Conf. (1976), EFI 76-55.
[14] D.J. Gross and F. Wilczek, Phys. Rev. D9 (1974) 980;
H. Georgi and H.D. Politzer, Phys. Rev. D9 (1974) 416.
[15] S. Stein et al., Phys. Rev. D12 (1975) 1884;
H.L. Anderson et al., Phys. Rev. Lett. 37 (1976) 4.
[16] M. Glück and E. Reya, Phys. Rev. D14 (1976) 3034.
[17] A. de Rujula, H. Georgi and H.D. Politzer, Phys. Letters 64B (1976) 428.
[18] H. Georgi and H.D. Politzer, Phys. Rev. D14 (1976) 1829.
[19] R.K. Ellis, R. Petronzio and G. Parisi, Phys. Letters 64B (1976) 97;
R. Barbieri, J. Ellis, M.K. Gaillard and G.G. Ross, Nucl. Phys. B117 (1976) 50.
[20] G. Donaldson et al., Phys. Rev. Letters 36 (1976) 1110.
[21] D.J. Gross, Phys. Rev. Letters 32 (1974) 1071.
[22] S.J. Brodsky and G.R. Farrar, Phys. Rev. Letters 31 (1973) 1153;
V. Matveev, R. Muradyan and A. Tavkhelidze, Nuovo Cim. Letters 7 (1973) 719.
[23] S.D. Drell and T.M. Yan, Phys. Rev. Letters 25 (1970) 316; Ann. of Phys. 66 (1971) 578.
[24] I. Hinchliffe and C.H. Llewellyn Smith, Phys. Letters B66 (1977) 281.
[25] I.G. Halliday, Nucl. Phys. B103 (1976) 343.
[26] J.H. Christenson et al., Phys. Rev. Letters 25 (1970) 1523; Phys. Rev. D8 (1973) 2016;
L.M. Lederman, Proc. 1975 Int. Symp. on lepton and photon interactions at high energies, Stanford, ed. W.T. Kirk (SLAC, 1976), p. 265.
[27] D.C. Hom et al., Phys. Rev. Letters 37 (1976) 1374;
L. Kluberg et al., Phys. Rev. Letters 37 (1976) 1451.
[28] Y. Afek, G. Berlad, G. Eilam, M. Glück and E. Reya, Technion preprint, PH-77-22.
[29] A.P. Contogouris, R. Gaskell and A. Nicolaidis, Large transverse momentum reactions in a parton model with logarithmic scale-breaking, McGill University report, 1977.
[30] S.M. Berman, J.D. Bjorken and J. Kogut, Phys. Rev. D4 (1971) 3388.